J Mater Sci: Mater Electron (2016) 27:5114–5120
DOI 10.1007/s10854-016-4402-z

Structural, magnetic and electrical transport properties of $Sm_{0.43}Nd_{0.10}Sr_{0.47}MnO_3$ thin film by DC-magnetron sputtering

S. Ramkumar[1] · G. Rajarajan[2] · H. K. Singh[3]

Received: 7 October 2015 / Accepted: 22 January 2016 / Published online: 30 January 2016

Abstract The paper contributes the preparation and characterization of $Sm_{0.43}Nd_{0.10}Sr_{0.47}MnO_3$ thin film. The thin film deposited on the single crystal of $LaAlO_3$ (001) substrates by DC-magnetron sputtering at 1053 K at a pressure of 200 m Torr. The deposited thin film was found to have insulating behavior when annealed in oxygen atmosphere at 1223 K for 24 h. The X-ray diffraction (XRD) study shows that, both 30 nm and 60 nm thin films reveal compressive strain. The magnetic measurement (M-H) shows that the paramagnetic to ferromagnetic transition temperature of 60 nm film is 145 K. At higher film thickness ($\sim$ 60 nm) a sharp insulator-to-metal transition is observed at 142 K ($T_{IM} = 142$ K). 60 nm film show a huge temperature co-efficient of resistance (TCR) and low field magneto resistance/an-isotropic magneto resistance (MR/AMR) is observed. The difference in the magneto transport properties of the two films have been explained in terms of presence of the magnetically and structurally disordered layer at the film-substrate interface.

✉ S. Ramkumar
ramkumarphd2015@gmail.com

[1] Department of Physics, Oxford Engineering College, Tiruchirappalli 620 009, Tamilnadu, India

[2] Department of Physics, Vidhya Mandhir Institute of Technology, Erode 638 052, Tamilnadu, India

[3] National Physical Laboratory (Council of Scientific and Industrial Research), Dr. K.S. Krishnan Marg, New Delhi 110 012, India

1 Introduction

The rich electronic phase diagram of the doped rare earth manganites ($RE_{1-x}AE_xMnO_3$, where RE = La, Nd, Sm, etc. and AE = Sr, Ca, Ba, etc.) is a natural consequence of the strong coupling between the mutually interacting spin, charge, orbital and lattice degrees of freedom [1, 23, 24, 28]. The phase diagram becomes more complex with the appearance of instabilities and phase inter diffusion, causing multicriticalilty with increasing size mismatch between the RE and AE cations. The compound $Sm_{1-x}Sr_xMnO_3$ by virtue of being close to the charge/orbital order (CO/OO) instability possesses intrinsic phase instabilities and multicritical points [23]. This low bandwidth (BW) compound shows variety of ground states such as (i) ferromagnetic metal (FMM) at $0.3 < x \leq 0.52$ (ii) antiferromagnetic insulator (AFMI) for $x > 0.52$ and (iii) for $0.4 < x \leq 0.6$, the charge ordering (CO) occurs with the ordering temperature (T_{CO}) increasing from $\sim$140 to 250 K as x increases in the above range. The competition between the FM, CO/OO, and AFM states becomes dominant near half doping ($x = 0.5$), and tri-critical peculiarities are observed in the x-dependent electronic phase diagram making $Sm_{1-x}Sr_xMnO_3$ an interesting candidate to study phase competition and related phenomena [10, 18, 19, 29]. Low field colossal magneto resistance (LF-CMR) is observed at all the compositions that corresponds to the FMM ground state in the range $0.3 < x \leq 0.52$. A first order transition from paramagnetic insulating (PMI) to the ferro magnetic metal (FMM) state is observed in $Sm_{1-x}Sr_xMnO_3$ ($x \sim 0.45$–0.50), which is technologically important for applications such as low temperature low field magneto resistive devices, bolometer and large magneto caloric effect (MCE) applications [19].

The low BW and strong phase coexistence/phase separation (PE/PS) also result in metamagnetism that provides intrinsic fragility to the composition-temperature (x-T) phase diagram vis-a-vis external perturbations. Consequently, even mild external perturbation such as electromagnetic field, pressure, lattice strain etc. provided by the substrate could dramatically modify their physical properties. Extensive investigations have been reported on $Sm_{1-x}Sr_xMnO_3$ (SSMO) in single- and poly- crystalline bulk forms. However, thin films of this compound, either polycrystalline or epitaxial have been studied for the first time [4, 6, 20].

Another important property of doped rare earth manganites is anisotropic magneto resistance (AMR) due to anisotropic magneto-crystalline nature that results in the dependence of resistivity on the angle between the applied magnetic field (**H**) and the direction of the transport current (**J**) [18]. The magnetic anisotropy is generally defined as the energy required to rotate the magnetization direction from the easy to the hard axis. Magneto crystalline anisotropy originates from the interaction between the electronic spin and orbital degrees of freedom. The electronic orbitals are linked to the crystallographic structure and their interaction with the spins aligns the latter preferentially along well defined crystallographic axes [20]. Therefore, there are directions in space, (generally referred to as the easy axis) along which a magnetic material is easier to magnetize in than in other ones. However, polycrystalline samples without a preferred granular orientation do not possess any magneto crystalline anisotropy. But, an overall isotropic behavior concerning the energy needed to magnetize it along any arbitrary direction is only given for a spherical shape. For non-spherical shapes there are one or more specific directions, solely caused by the shape which represents easy magnetization axes [13]. This anisotropy is known as shape anisotropy. The direction of magnetization is determined by the competing magneto crystalline and shape anisotropies. The constant characterizing magneto crystalline anisotropy is found to be smaller than that characterizing the shape anisotropy and hence the later dominates the former which results in an in-plane magnetization in thin films. In low dimensional systems such as thin films, the anisotropies are affected further by the broken symmetry at the interfaces and hence additional contributions that are forbidden in three dimensional cases arise. In manganite thin films the non-spherical charge distribution around Mn ions gets further modified by substrate induced strain and lattice defects. Apart from the strain and hence the film thickness other factors such as structural defects, spin disorder, nature of the magnetic ground state, phase coexistence, etc. are also expected to play a crucial role. The occurrence and nature of the low field AMR in low bandwidth manganites with strong phase coexistence such as $Sm_{1-x}Sr_xMnO_3$ (SSMO) has not been given much attention. In the present work we have studied the variation of LF-MR as a function of the angle (θ) between the applied magnetic field (**H**) and current applied (**J**) in the plane of the film. Huge anisotropy is observed in magneto transport.

Partial replacement of smaller Sm^{3+}cations by larger cations (like Nd^{3+}) increases the average A-site cationic radius and hence increases the BW. The paramagnetic-ferromagnetic (PM-FM) and insulator-metal transition temperatures (T_C/T_{IM}) are expected to be enhanced as compared to the Nd free compound [1, 23]. In the previous study [25], authors have prepared $Sm_{0.45}Nd_{0.08}Sr_{0.47}MnO_3$ thin-film and carried out detailed study of micro structural and magneto transport properties. Thin films thickness ~36 and ~80 nm were grown by DC magnetron sputtering on LAO (001) substrate and post-annealed in oxygen atmosphere. The results clearly explain that extremely large compressive strain broadens the PMI-FMM transition in the as-grown films. O_2 annealing relive the strain, which causes a phase-separated meta magnetic ground state showing field induced first-order phase transition (AFM-COI) at ~36 nm film. At higher film thickness ~80 nm, the degree of phase separation is reduced and a zero field PMI-FMM transition, with a weak first-order phase separation is observed. This result also suggests that the compressive stain does not always favor FMM phase, but its relaxation is certainly obstruct to the AFM-COI. In the present paper, the investigation is carried out on the impact of thickness on structure and magneto transport property in single crystalline $Sm_{0.43}Nd_{0.10}Sr_{0.47}MnO_3$ (SNSMO) thin films prepared by DC magnetron sputtering and the results are reported.

In the present paper, three different studies have been conducted. Namely, Temperature coefficient of resistivity with temperature (TCR), An-isotropic Magneto resistance (AMR) and Plot of T^{-1} versus ln (ρ/T) corresponding to the 30–60 nm films are estimated and compared with the experimental data.

From the TCR graph, the sharpness of the IMT was evaluated and is found to be 83 % at T = 139 K (60 nm film).The MR and AMR (at H = 4.5 KOe) was calculated and found to be ~69 and ~−65 %, respectively. It shows a peak at T = 139 K in the vicinity of T_{IM} (60 nm film).

From the slope of T^{-1} versus ln (ρ/T) plot, to measure the activation energy E_A. In 30 nm film, shows the value of activation energy is appreciable large than that of 60 nm film, In 30 nm film T_{IM} (~130 K) is observed to decrease with increasing activation energy (E_A = 122.3 meV). The higher value of E_A shows that the carriers are strongly localized than the thicker film. This could be due to the presence of higher degree of disorder due to large substrate-induced compressive strain, oxygen vacancies etc.,

For 60 nm film, T_{IM} (~145 K) is measured to increase with decreasing activation energy (E_A = 99.9 meV). This suggested that J-T effect has appreciably softened and this is brought about by the out-plane compressive strain and they have higher value of FMM fraction. The variation of E_A as function of film thickness.

2 Experimental detail

The sputtering target was prepared from $Sm_{0.43}Nd_{0.10}Sr_{0.47}MnO_3$ (SNSMO) powders synthesized by a wet chemical route. High purity (99–99.99 %) metal nitrates, viz., $Sm(NO_3)\cdot 6H_2O$, $Nd(NO_3)\cdot 6H_2O$, $Sr(NO_3)_2$ and $Mn(NO_3)_2\cdot 4H_2O$, were dissolved in 200 ml of de-ionized water and an equal volume of ethylene glycol was added. The mixture was heated at 373 K with constant stirring until a resin was formed. This resin was decomposed at 573 K and finely crushed. The resultant powder was vigorously mixed and then heated for 12 h at 973 K to get a highly homogenized SNSMO powder for the target. The target was sintered at 1373 K for about 24 h. The lattice constants of the target material are a = 5.452, b = 5.443 and c = 7.684 Å. The average grain size was determined from surface morphological investigations by SEM to be ~500 nm. The detailed wet chemical process is given elsewhere [8, 9, 17]. Films with thicknesses in the range 30–60 nm were deposited by on-axis DC-magnetron sputtering of 2″ $Sm_{0.43}Nd_{0.10}Sr_{0.37}MnO_3$ (SNSMO) target on the single-crystal $LaAlO_3$ (001) substrates maintained at 1053 K at a dynamic pressure of 200 mtorr of Ar (80 %) + O_2 (20 %). The grown films were found to be insulating and therefore were annealed in flowing oxygen at 1223 K for 12–24 h. The structure/microstructure was characterized by powder X-ray diffraction (θ–2θ and ω-scans) and the cationic composition was studied by energy dispersive spectroscopy (EDS). Temperature and magnetic field dependent magnetization was measured by using commercial physical property measurement systems (PPMS-Quantum Design) and the electrical transport was measured by standard four probe method in the temperature range 77–300 K.

3 Results and discussion

In the following sections the structural and magneto transport properties of 30–60 nm thin films are described in detail. The authors have also attempted to correlate the magneto transport properties of these films to the structural characteristics.

4 Structure

The lattice constants of the target material are a = 5.452, b = 5.443 and c = 7.684 Å. The average grain size was determined from surface morphological investigations by SEM to be ~500 nm. This yields the average in-plane and out-of-plane cubic lattice constants, a_C^{in} = 3.852 and a_C^{out} = 3.842 Å, respectively. LAO (a_S = 3.798 Å) possesses smaller lattice constant than a_c^{in} of the target bulk compound [1, 23, 24]. Hence, the films on LAO are expected to grow under compressive strain ($\varepsilon \approx -1.4$ %). Here, the compressive strain has been defined as $\varepsilon = (a_S - a_C^{in})*100/a_C^{in}$. The X-ray diffraction (XRD, θ–2θ scan) pattern of the 30–60 nm thin films are shown in Fig. 1. The occurrence of only the (00ℓ) diffraction maxima shows that the films have grown along the out of plane (c-axis) direction. The out of plane cubic lattice constants estimated from the X-ray diffraction data are a_C = 3.939–3.867 Å, respectively, for 30–60 nm films. The out of plane lattice parameters of both the 30–60 nm films are larger than the out-of-plane lattice parameter of the bulk target used. This clearly shows that both the films are under compressive strain [16, 22, 26]. The much larger out-of-plane lattice constant of the 30 nm film than that of the 60 nm film reveals that the former is under higher degree of compressive strain. As the film thickness increases the strain relaxes gradually and the out-of-plane lattice parameter approaches towards the bulk value. This is well demonstrated by the smaller out-of-plane lattice parameter of the thicker 60 nm film. In manganites the strain is known to influence the magneto-electronic phases in a very profound manner. The tensile strain is believed to favor the COI-AFM phase while the compressive strain enhances the FMM fraction. The compressive strain results in an elongation of the MnO_6 octahedra in the out-of-plane direction with a concomitant compression in the basal plane (in the present case in the plane

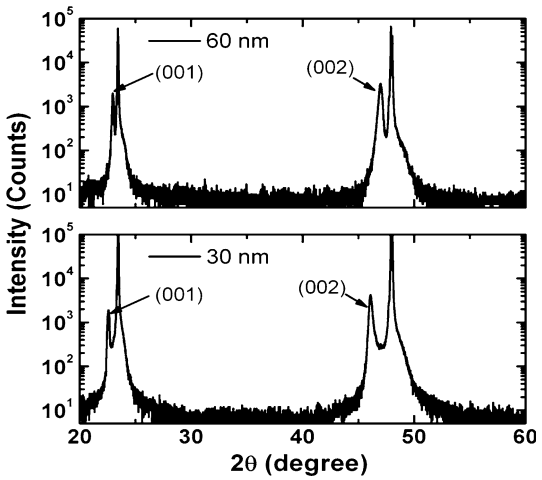

Fig. 1 The XRD pattern of the 30 nm and 60 nm thin films on LAO (001) substrates. The larger intensity peaks belong to the substrate and the indexed ones belong to the SNSMO

substrate) that causes a reduction in the degree of Jahn–Teller distortion, and hence weakens the spin-lattice coupling [12, 22, 27]. On the other hand the tensile strain elongates the MnO_6 octahedra in the basal plane with a concomitant compression along the out-of-plane direction.

4.1 Magnetic properties

The temperature dependent zero field cooled (ZFC) and field cooled (FC) magnetization data (M(T)) taken at H = 500 Oe is shown in Fig. 2 for 60 nm film. The PM-FM transition temperature (T_C) is 145 K. The $M_{ZFC}(T)$ and $M_{FC}(T)$ curves show strong divergence at $T \approx 125\ K < T_C$. The M-H data (taken at 5 K) of these films is presented in the inset of Fig. 2. The saturation magnetization (M_S) ≈ 7.94 emu and the corresponding saturation field is $H_S \approx 6$ kOe. The remnant magnetization (M_r) is ≈ 2.9 emu and the coercivity is $H_{C-} = -3.2$ kOe and $H_{C+} = 2.3$ kOe. In the lower temperature regime, the ZFC curve shows a decline which however vanishes in the FC magnetization curve [1]. Generally, ZFC-FC magnetization divergence and the drop in ZFC magnetization at $T < T_P$ are regarded as signatures of a metamagnetic state. The nature of the bifurcation of these curves suggests that in the present case the metamagnetic state could be either a cluster glass or spin glass [11, 22, 23]. The occurrence of the cluster glass or spin glass state in manganites is generally attributed to the coexistence of AFM-COI phases in the FMM matrix. In the present case (i) long range FMM, (ii) short range CO/OO-AFMI phases and (iii) short range A-AFM phases are expected to coexist at $T < T_C$. It is this phase-coexistence that results in meta magnetism and the formation of the CG at $T < T_C$. The ZFC-FC M-T data of the as grown 30 nm film was observed to be noisy and showed a broad PM-FM transition [25]. The lower film thickness is very difficult to pick up even by the SQUID magnetometer. This makes the M-T data of the as- grown films noisy.

4.2 Electrical transport properties

The temperature dependence of resistivity measured in the range 77–300 K is shown in Fig. 3. The 30 nm thin film shows insulator like temperature dependence throughout the measurement's temperature range. This is in contrast to the bulk target used for the deposition of these films [30]. The target showed an insulator metal transition (IMT) at $T_{IM} \approx 130$ K [3, 25]. In the 60 nm thin film the lowering of temperature results in an insulator like behavior but it shows a very sharp IMT at $T_{IM} = 142$ K. The observed value of T_{IM} is higher than that of the Nd free material, viz., $Sm_{0.53}Sr_{0.47}MnO_3$. Just below the IMT, the resistivity decreases by almost three orders of magnitude with in a very small temperature range [11, 12]. The sharpness of the IMT was evaluated by the temperature coefficient of resistivity defined by $d(\ell n\rho)/dT$. The TCR (%) is found to be 83 % at T = 139 K (shown in Fig. 4). This value of TCR is considerably larger than that of the large and intermediate bandwidth manganites such as $La_{1-x}Sr_xMnO_3$ ($x = 0.2$–0.4) and $La_{1-x}Ca_xMnO_3$($x = 0.3$-0.4), which is generally in the range 5–20 %. The sudden drop in the resistivity at IMT is generally attributed to the bicritical nature of the low bandwidth manganites. At $T > T_{IM}/T_C$ the major phase is paramagnetic insulator (PMI). However, it has been shown that antiferro magnetically charge ordered insulator (AFM-COI) clusters may be present or embedded in the PMI matrix. This is well evident by the

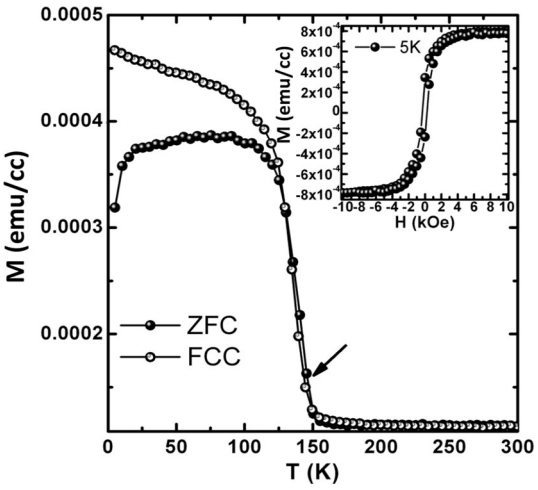

Fig. 2 Temperature dependent zero field cooled (ZFC) and field cooled (FC) magnetization (H@ 500 Oe) for 60 nm film. The *inset* shows M-H loop measured at 5 K

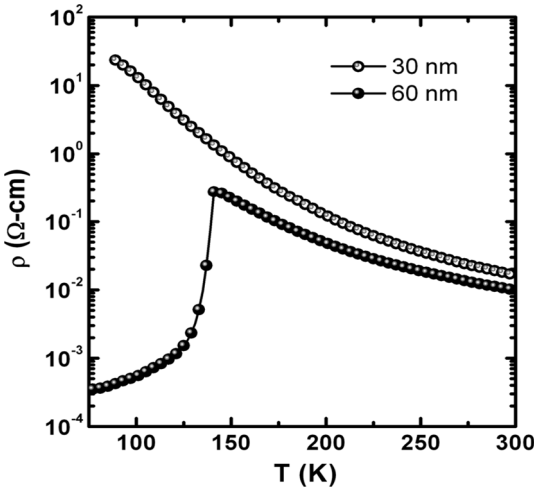

Fig. 3 The variation of zero magnetic field resistivity with temperature measured in the range 77–300 K

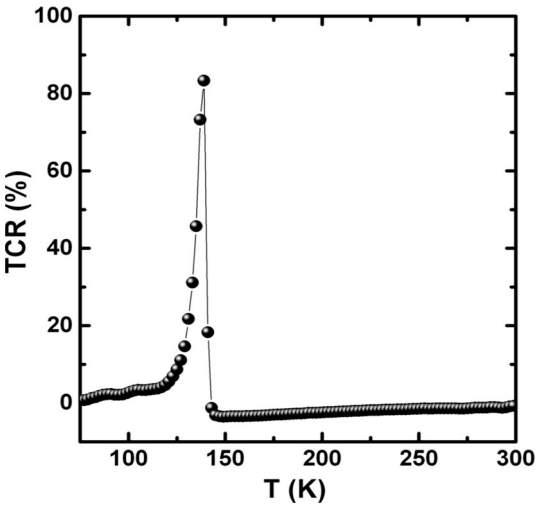

Fig. 4 Variation of the temperature coefficient of resistivity with temperature for the 60 nm film

sharp rise in resistivity just above IMT [5, 11]. At the IMT the FMM phase appears abruptly with concomitant collapse of the PMI phase, causing the sharp IMT.

Borges et al. [2] has been proposed the concept of the presence of magnetically dead layers to account for the anomalous features in the magnetic and magneto transport properties of manganite thin films. Two magnetically dead layers are present at both the film substrate interface and the film surface. The magnetization rapidly falls off inside these interfaces due to spin canting, which induces loss of polarization. This loss of magnetic polarization has been confirmed by spin-resolved photoemission spectroscopy [8, 14]. The temperature dependence of the moment at the surface exhibits a markedly different behavior from that of the bulk magnetization. Further, the universality of the "dead layer" is not well established. It was shown that the concept of dead layers is not always applicable and is too simple to capture the physics of manganites. The magnetic and transport properties of manganite films are dependent on the annealing conditions, that is, whether the films are annealed ex situ or in situ. It has also been theoretically shown that magnetic and transport properties depend on the degree of tetragonal distortion as well as on different strain states induced by the different annealing procedures [7, 12, 31]. It is also known that the breaking of the Mn^{4+}–O–Mn^{3+} network chain near the film-substrate interface causes induced phase separation. This can cause a small deviation from the nominal Mn^{4+}/Mn^{3+} ratio in the vicinity of the interface. Furthermore, as ultra-thin films are supposed to be under a large degree of substrate-induced strain, some chemical nonstoichiometry and interfacial oxygen vacancies are also possible. As the film thickness increases, these are stabilized. Thus, interface-induced phase separation leads to the creation of a magnetically disordered and chemically inhomogeneous state in the vicinity of the film-substrate interface, whose contribution is more prominent at lower film thicknesses. In view of this we attribute the insulator like ρ-T of the 30 nm thin films to the presence of a disordered layer at the film substrate interface. As the film thickness increases the substrate-induced strain, some chemical nonstoichiometry [3], interfacial oxygen vacancies [8, 25], etc. are stabilized and the impact of this disordered layer is suppressed. Hence, the thicker 60 nm films show a sharp IMT.

As mentioned earlier *JT* distortion of the MnO_6 octahedron can lead to the trapping of the charge carriers into a polaronic state influencing the transport properties in the high temperature *PM* phase. Hence, the temperature dependence of resistivity data above T_C/T_{IM} is an important probe of the conduction mechanism. In manganite thin films, strong polaronic effect is expected at $T > T_{IM}$. We have investigated the resistivity of 30 nm and 60 nm SNSMO films in the above temperature regime in the framework of the Emin–Holstein approach of small polaron hopping in the adiabatic limit given by the expression

$$\rho(T) = AT\exp(E_A/K_BT) \text{ where } A = 2k_B/3ne^2a^2v$$

Here, '*n*' is the polaron concentration; '*a*' is the site-to-site hopping distance, '*v*' the attempt frequency and k_B is the Boltzmann constant. E_A is the activation energy, i.e., the height of the potential barrier and $E_A = E_P/2\text{-}t$. In general, the overlap integral *t* is so small that it could be neglected and then $E_A \approx E_P/2$ or the polaron binding energy $E_P \approx 2E_A$. In Fig. 5, ln(ρ/T) is plotted against inverse of temperature (*1/T*) and the linearity is observed at $T > T_{IM}$. The solid lines in the plot are linear fit to the experimental data [11, 21]. The authors calculated the activation energy, E_A from the fitting parameter [16, 23].

The above law nicely fits the experimental data in the range 150–300 K for both 30 nm and 60 nm films. The T^{-1} vesus ln(ρ/T) plot for both the films is shown in Fig. 5. From the fitting parameter [slope of the T^{-1}vs. ln(ρ/T) plot], we estimated the activation energy. The value of the activation energy was found to be E_A = 122.3–99.9 meV, respectively, for 30 and the 60 nm films. For the 30 nm film, the value of E_A is appreciably larger than that of the 60 nm film. This could be due to the presence of higher degree of disorder due to large substrate-induced strain, some chemical non-stoichiometry, interfacial oxygen vacancies, etc. in the 30 nm films. The higher value of E_A in the 30 nm film shows that the carriers are more localized than in the 60 nm film.

The temperature and magnetic field dependent electrical resistivity was measured by the standard four probe technique. The magneto resistance (*MR*) is defined as $100*\Delta\rho/\rho(0)$, where $\Delta\rho = \rho(0)–\rho(H)$ was measured at magnetic

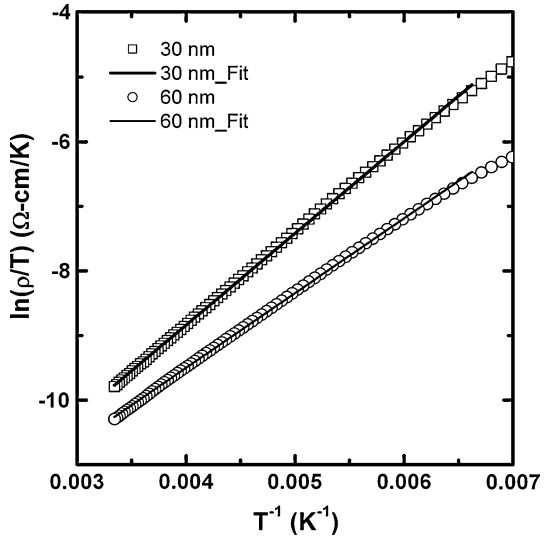

Fig. 5 T^{-1} versus ln (ρ/T) plot at $T > T_{IM}$ corresponding to the 30–60 nm SNSMO films. The *open symbols* represent the measured data while the *solid lines* are fit to the experimental data

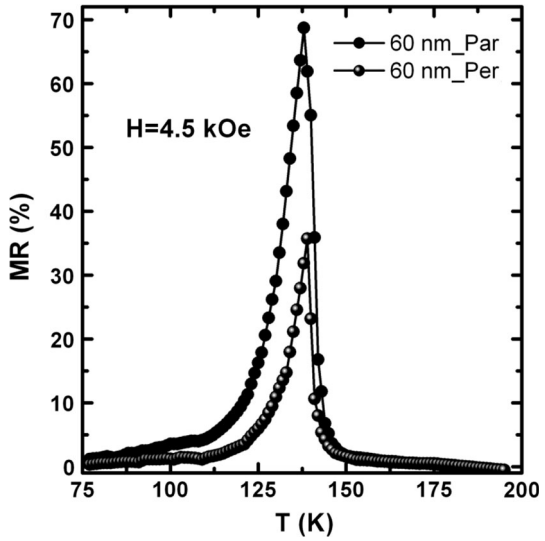

Fig. 7 Temperature dependence of MR for 60 nm thin film measured with **H//J** (*solid circles*) and **H⊥J** (*solid spheres*)

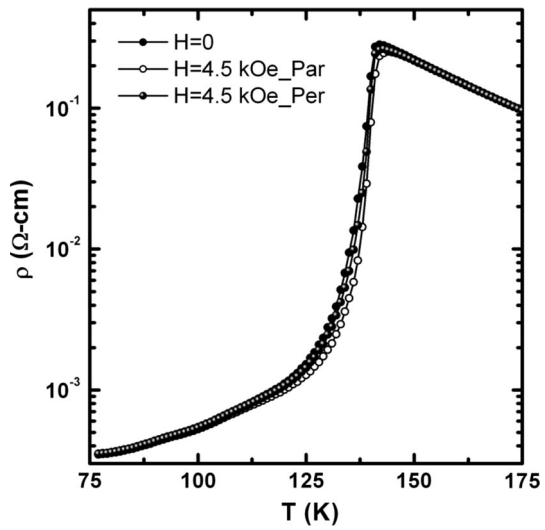

Fig. 6 The temperature dependent of resistivity of the 60 nm film measured at zero magnetic field (*solid circles*), applied magnetic field H = 4.5 kOe, with **H//J** (*open circles*) and **H⊥J** (*solid spheres*)

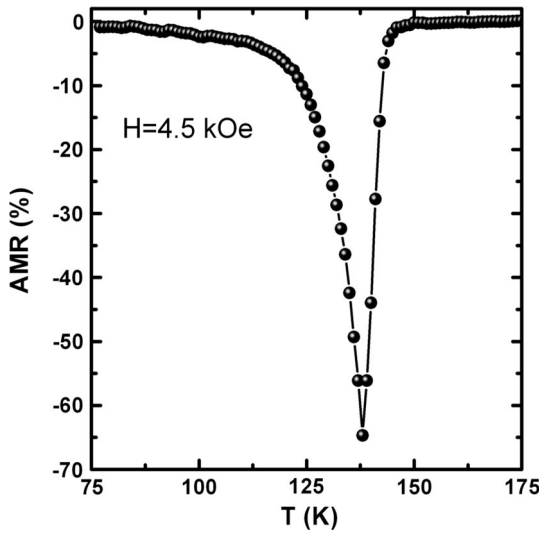

Fig. 8 Temperature dependence of the AMR for 60 nm thin film measured at H = 4.5 kOe

field H = 4.5 kOe. The temperature dependent resistivity of the SNSMO films was also measured as a function of the angle (θ) between **H** and the direction of the current **J**. From these measurements the anisotropic magneto resistance (AMR) was calculated [13, 15, 26]. The AMR measured in the present study defined as AMR = $(\rho_{\parallel}^{in}-\rho_{\perp}^{out})*100/\rho_{av}$. $\rho_{\parallel}^{in}$ is the resistivity of the film for **H** located in the plane of the film and oriented parallel to **J**. $\rho_{\perp}^{out}$ represents the resistivity measured when **H** is applied perpendicular to both the plane of the film and the current **J**. The average resistivity is defined to be $\rho_{av} = \rho_{\parallel}^{in}/3 + 2\rho_{\perp}^{out}/3$. All the measurements were carried out in the temperature range 77–300 K and the maximum **H** was 4.5 kOe. The 30 nm film did not show significant MR and AMR in the measured temperature range. Both, MR and AMR were less than 2 % at 77 K/4.5 kOe and rapidly vanished on increasing the temperature [1, 16, 23]. The temperature dependent of resistivity of the 60 nm film measured at applied magnetic field H = 4.5 kOe, with **H//J** and **H⊥J** are shown in Fig. 6. The 60 nm film showed a huge low field MR ~69 % when the current is applied parallel to the magnetic field (**H//J**). The MR decreases drastically to ~35 % when the applied magnetic field is

made perpendicular to the transport current ($\mathbf{H}\perp\mathbf{J}$) as shown in Fig. 7. The AMR (at H = 4.5 kOe) was calculated using the above expression and was found to be AMR ~ -65 % (Fig. 8). The MR and AMR showed a peak at T = 139 K.

5 Conclusions

Thin films of $Sm_{0.43}Nd_{0.10}Sr_{0.47}MnO_3$ (SNSMO) have been successfully grown on single crystal LAO (001) substrates by DC magnetron sputtering. Impact of the film thickness on the structure and magneto transport has been investigated. At lower film thickness ($\sim$30 nm) the SNSMO films have insulator like characteristics, significantly larger small polaron activation energy and show negligible magneto resistance. The PM-FM transition temperature (T_C) of $\sim$60 nm film is $T_C = 145$ K. At higher film thickness ($\sim$60 nm), the carriers are delocalized resulting in a sharp insulator to metal transition is observed at $T_{IM} = 142$ K. The thicker (60 nm) film shows a huge TCR and low filed MR/AMR in the vicinity of T_{IM}. The observed difference in the magneto transport properties of the two films has been explained in terms of the presence of the magnetically and structurally disordered layer at the film substrate interface.

Acknowledgments SR is thankful to Indian Academy of Sciences, Bengaluru for Summer Research Fellowship and National Physical Laboratory (CSIR), New Delhi for the research facilities.

References

1. V. Agarwal, R. Prasad, M.P. Singh, P.K. Siwach, A. Srivastava, P. Fournier, H.K. Singh, Appl. Phys. Lett. (2010). doi:10.1063/1.3302455
2. R.P. Borges, W. Guichard, J.G. Lunney, J.M.D. Coey, F. Ott, J. Appl. Phys. (2001). doi:10.1063/1.1331658
3. E. Breckenfeld (2014) Growth-induced non-stoichiometry in complex oxide Systems. Ph.D Dissertation, University of Illinois at Urbana-Champaign
4. M. Egilmez, K.H. Chow, J. Jung, Z. Salman, Appl. Phys. Lett. (2007). doi:10.1063/1.2724906
5. M. Egilmez, R. Patterson, K.H. Chow, J. Jung, Appl. Phys. Lett. (2007). doi:10.1063/1.2746956
6. M. Egilmez, K.H. Chow, J. Jung, I. Fan, A.I. Mansour, Z. Salman, Appl. Phys. Lett. (2008). doi:10.1063/1.2904699
7. M. Gezlaff, Phys. Rev. Lett. (2008). doi:10.1103/102.077205
8. A.M. Haghiri-Gosnet, J.P. Renard, J. Phys. D Appl. Phys. (2003). Available at stacks.iop.org/JPhysD/36/R127
9. M. Kasai, H. Kuwahara, Y. Tomioka, Y. Tokura, J. Appl. Phys. (1996). doi:10.1063/1.363759
10. C. Martin, A. Maignan, M. Hervieu, B. Raveau, Phys. Rev. B (1999). doi:10.1103/PhysRevB.60.12191
11. J.A. Mydosh, *Spin Glasses: An Experimental Introduction*, 2nd edn. (Taylor & Francis, London, 1993)
12. J. O'Donnell, J.N. Eckstein, M.S. Rzchowski, Appl. Phys. Lett. (2000). doi:10.1063/1.125707
13. H. Oshima, K. Miyano, Y. Konishi, M. Kawasaki, Y. Tokura, Appl. Phys. Lett. (1999). doi:10.1063/1.124729
14. J.-H. Park, E. Vescovo, H.-J. Kim, C. Kwon, R. Ramesh, T. Venkatesan, Phys. Rev. Lett. (1998). doi:10.1103/PhysRevLett.81.1953
15. R. Patterson, C. Ozeroff, K.H. Chow, J. Jung, Appl. Phys. Lett. (2006). doi:10.1063/1.2199594
16. R. Prasad, M.P. Singh, P.K. Siwach, W. Prellier, A. Kaur, H.K. Singh, J. Appl. Phys. (2008). doi:10.1063/1.2902927
17. W. Prellier, P.H. Lecoeur, B. Mercey, J. Phys.: Condens. Matter. (2001). doi:10.1088/0953-8984/13/48/201
18. A. Rebello, R. Mahendiran, Appl. Phys. Lett. (2008). doi:10.1063/1.3040698
19. C. Reitz, P.M. Leufke, R. Schneider, H. Hahn, T. Brezesinski, Chem. Mater. (2014). doi:10.1021/cm5028282
20. P. Sarkar, P. Mandal, P. Choudhury, Appl. Phys. Lett. (2008). doi:10.1063/1.2919732
21. G. Singh-Bhalla, S. Selcuk, T. Dhakal, A. Biswas, A.F. Hebard, Phys. Rev. Lett. (2009). doi:10.1103/PhysRevLett.102.077205
22. M.K. Srivastava, P.K. Siwach, A. Kaur, H.K. Singh, Appl. Phys. Lett. (2010). doi:10.1063/1.3505327
23. M.K. Srivastava, M.P. Singh, P.K. Siwach, A. Kaur, F.S. Razavi, H.K. Singh, Solid State Commun. (2012). doi:10.1016/j.ssc.2011.10.023
24. M.K. Srivastava, S. Singh, P.K. Siwach, A. Kaur, V.P.S. Awana, K.K. Maurya, H.K. Singh, AIP Adv. (2013). doi:10.1063/1.4805077
25. M.K. Srivastava, S. Singh, P.K. Siwach, K.K. Maurya, V.P.S. Awana, A. Kaur, H.K. Singh, Mater. Res. Express (2014). doi:10.1088/2053-1591/1/1/016110
26. P.A. Stampe, H.P. Kunkel, Z. Wang, G. Williams, Phys. Rev. B (1995). doi:10.1103/PhysRevB.52.335
27. Y. Suzuki, H.Y. Hwang, S.W. Cheong, R.B. Van Dover, Appl. Phys. Lett. (1997). doi:10.1063/1.119454
28. Y. Tokura, Rep. Prog. Phys. (2006). doi:10.1088/0034-4885/69/3/R06
29. Y. Tomioka, H. Hiraka, Y. Ended, Y. Tokura, Phys. Rev. B (2006). doi:10.1103/PhysRevB.74.104420
30. H.S. Wang, Q. Li, Appl. Phys. Lett. (1998). doi:10.1063/1.122461
31. M. Ziese, Phys. Rev. B (2000). doi:10.1103/PhysRevB.62.1044